npj | climate and atmospheric science

Article

Published in partnership with CECCR at King Abdulaziz University

https://doi.org/10.1038/s41612-024-00618-0

The prevalent life cycle of agricultural flash droughts

Miguel A. Lovino[1,2] ✉, M. Josefina Pierrestegui[1,2], Omar V. Müller[1,2], Gabriela V. Müller[1,2] & Ernesto H. Berbery[3]

This work examines the characteristics and prevalent life cycle of agricultural flash droughts globally. Using ERA5 data, the study introduces a flash drought indicator based on soil water availability. This approach integrates root-zone soil moisture and hydraulic soil properties, such as field capacity and wilting point, to couple the rapid soil moisture depletion and plant water stress. Our findings reveal that agricultural flash droughts present their higher frequency predominantly during the critical growth periods of crops. Notably, these droughts exhibit a similar life cycle regardless of the location or climatic regime. The primary cause of the rapid soil moisture depletion is the precipitation deficit, but evapotranspiration also plays a significant role. In an energy-limited environment, evapotranspiration rapidly increases before the onset and decreases rapidly during the intensification period as the system becomes water-limited. Upon concluding the intensification period, most crops experience water stress, diminishing their yields.

Flash droughts, characterized by the rapid drying of soils over durations lasting weeks to a couple of months[1,2], have become more common than slow droughts over much of the world since the 1950s[3]. The frequency and severity of flash droughts are projected to increase worldwide during the 21st century, especially over croplands under high global warming scenarios[4,5]. Given their rapid onset and intensification, flash droughts are often unexpected and challenging to predict[6]. They can negatively impact crop yields in agricultural regions and damage natural ecosystems worldwide[7–9].

Agricultural flash droughts affect vegetation when there is a soil moisture deficit and plant water requirements are not met, especially during the critical growth period of crops. The primary forcings are precipitation deficits and positive temperature anomalies that favor rapid soil moisture depletion rates[2,10,11]. Soil moisture can be considered a proxy representing the moisture state of the land-atmosphere system as it dominates dryness stress on vegetation productivity across most of the world's vegetated land areas[12]. Thus, plants with shallow roots, such as crops and pastures, are sensitive to soil moisture deficits in the upper soil layer and can become moisture-stressed faster than plants with deep roots[11]. Hence, rapid soil moisture depletion is expected to impact crops and grasslands more severely than forests[13].

Any attempt at predicting flash droughts requires a better understanding of their evolution and life cycle. During the evolution of flash droughts, precipitation rapidly decreases, playing a key role in the rapid soil moisture depletion[10,14]. Case studies show that the coevolution of anomalous meteorological conditions, such as high evaporative demand and temperatures, favor the development and propagation of flash droughts[11,15–17]. Land-atmospheric coupling also accelerates flash drought onsets[18,19].

The main flash drought drivers have been studied at the regional and global scales[14,20–22] employing different indicators[23] primarily based on soil moisture variability[24–26], the evaporative stress ratio[27], evaporative demand[28], or multivariate approaches[14,15,29]. The variety of definitions responds to specific needs, as flash drought physical processes are complex and difficult to represent using a single definition. However, different classifications may produce diverse results regarding flash drought characteristics and key drivers[30,31].

As highlighted by ref. 31, a crucial aspect of flash drought development involves coupling rapid depletion rates of soil moisture in the root zone with impacts on vegetation health. To this end, we propose a flash drought indicator that relies on soil water availability and can integrate the dominant physical processes with the corresponding effects on vegetation health, mainly for agricultural regions. Using this method, this study assesses the prevalent life cycle of agricultural flash droughts, highlighting global similarities. We analyze atmospheric and surface drivers throughout this cycle and discuss the impact of these droughts during the critical growth period of crops.

[1]Consejo Nacional de Investigaciones Científicas y Técnicas (CONICET), Santa Fe, Argentina. [2]Centro de Estudios de Variabilidad y Cambio Climático (CEVARCAM), Facultad de Ingeniería y Ciencias Hídricas (FICH), Universidad Nacional del Litoral (UNL), Ciudad Universitaria, Ruta Nacional N° 168 - km 472,4. (3000), Santa Fe, Argentina. [3]Earth System Science Interdisciplinary Center/Cooperative Institute for Satellite Earth System Studies, University of Maryland, College Park, College Park, MD 20740, USA. ✉e-mail: mlovino@unl.edu.ar

Results

Overview of the proposed method to detect agricultural flash droughts

Soil moisture (θ) is a crucial variable for monitoring the stress of the land system[10,32]. Its conditions reflect the actual water availability for plants while considering the time-integrated impact of preceding meteorological states that affect the soil wetness (e.g., precipitation, solar radiation, and wind speed). A soil moisture deficit limits direct soil evaporation, water uptake by roots for plant transpiration, and groundwater recharge[33]. The decreased soil moisture and the corresponding increase in evaporative demand induce plant water stress[2]. The soil moisture deficit and plant water stress can be explained through the hydraulic properties of the soil, specifically the field capacity (θ_{FC}) and the permanent wilting point (θ_{WP}). Soil cannot retain water above the field capacity because gravitational drainage predominates in the soil matrix. Plants cannot use soil moisture below the wilting point because the soil matrix holds water too tightly around the soil particles[32,34]. Consequently, the maximum amount of water that soil can store and provide for plant growth and transpiration is the available water capacity ($\theta_{AWC} = \theta_{FC} - \theta_{WP}$) (see, e.g., ref. 35 for further details).

Building from these principles, ref. 36 defined the Soil Water Deficit Index (SWDI) as an agricultural drought index formulated as:

$$\mathrm{SWDI} = \left(\frac{\theta - \theta_{FC}}{\theta_{FC} - \theta_{WP}}\right) \times 10 \quad (1)$$

The SWDI equals zero when the soil moisture is at the field capacity, i.e., when plants have full water availability and no soil moisture deficit. Negative SWDI values indicate a soil moisture deficit, which becomes absolute when $\theta \le \theta_{WP}$ (SWDI ≤ -10). Below this point, there is no available water for plants, i.e., roots cannot absorb soil water, and plants wilt[37].

The critical soil moisture value[32,38] (θ_{CRIT}), an essential threshold lying between θ_{WP} and θ_{FC}, differentiates evapotranspiration regimes (see Fig. 1a adapted from refs. 10,32; and Supplementary Fig. 1): When $\theta > \theta_{CRIT}$, evapotranspiration is independent of soil moisture (energy-limited regime). When $\theta < \theta_{CRIT}$, evapotranspiration is constrained by soil moisture (water-limited regime). Thus, θ_{CRIT} occurs at the point when evapotranspiration becomes water-limited and is identified when a slight decrease in soil moisture leads to diminished evaporative fraction (the ratio of latent heat to the combined latent and sensible heat fluxes)[32,38]. A transitional regime corresponds to the range $\theta_{WP} \le \theta \le \theta_{CRIT}$, where soil moisture limits evapotranspiration and, thus, land-atmosphere feedback. The system is in a dry regime when no evapotranspiration can occur, that is, when $\theta < \theta_{WP}$ (or SWDI < -10, Fig. 1a).

The proposed approach considers fundamental characteristics of a flash drought (e.g., refs. 2,3,10,24): (1) a rapid depletion of the root-zone soil moisture, (2) an intensification period sufficiently long to avoid short synoptic scale events that deplete soil moisture rapidly but recover suddenly, (3) reasonably unstressed soil moisture conditions prior to drought onset, and (4) plant water stress. First, the rapid decay of the soil moisture is represented by an SWDI decay from more than −3 to less than −5 in 20 days (or 4 pentads) (see Fig. 1b). The SWDI thresholds are based on the following refs. 10,32,39,40 that have addressed the relationship between soil moisture and evapotranspiration. The upper threshold (SWDI = −3), at the beginning of the transitional regime, guarantees a discernible decrease in evapotranspiration and thus effectively identifies a level of moisture deficit within the land system. The lower threshold (SWDI = −5) ensures that plants begin to experience water stress (see further details on Methods). Second, the minimum duration of the intensification period is met (following ref. 25) by requiring the soil moisture depletion period to last at least 15 days (or three pentads). Third, the non-drought condition prior to the drought onset is fulfilled (adapted from ref. 10) by requiring the three pentads preceding an event to exhibit SWDI values higher than −4 in magnitude. It also prevents flash droughts to overlap in time when, following the conclusion of a flash drought due to partial soil moisture recovery from a precipitation event, rapid soil moisture depletion takes place due to preceding conditions. Fourth, the plant water stress is intrinsically integrated into the proposed indicator, as it directly addresses the water availability loss for plants by defining the SWDI thresholds.

With a primary focus on crops, the proposed definition couples the rapid intensification of soil moisture drying and vegetation stress as crucial factors. Therefore, the method targets agricultural flash droughts—that is, specifically those occurring in areas prone to agriculture—rather than all instances of flash droughts. Notably, agricultural flash droughts are rare in regions with extreme climates (see Methods for details). Furthermore, the proposed approach does not remove the annual soil moisture cycle. Then, it is expected that the higher soil moisture decreases will occur during the growing season (mainly in spring and extending into summer) when soil moisture is largely influenced by increases in evapotranspiration rates that exacerbate precipitation deficits. Thus, aligning with their definition, agricultural flash droughts are susceptible to occur during the growing season regardless of the climatic regime.

Representation of well-known historical flash droughts

The proposed method is implemented using the European Centre for Medium-Range Weather Forecasts reanalysis version 5 (ERA5) data. This method, focused on characterizing agricultural flash drought by tracking the spatiotemporal evolution of the SWDI (as illustrated in Fig. 2), effectively identifies the prevalent pattern of the well-documented 2012 flash drought in the central-eastern United States[11,30,41,42] that severely impacted agriculture[43]. The agricultural flash drought began to develop rapidly in late April towards the north of the southeastern region (Fig. 2f, b, g). Throughout late May and June, the agricultural flash drought expanded in a radial pattern with varying rates of intensification (Fig. 2f, c, h, d, i). By July it reaches its maximum spatial extent, spreading further into the northern States of the Midwestern region (Fig. 2e, j). Agricultural flash drought conditions do not develop towards the semi-arid regions west of 100° W and the desert areas of the Southwest USA (Fig. 2f), as they show low SWDI values (SWDI < −7, and SWDI < −10, respectively) but constant over time (Fig. 2a–e).

We also assess the robustness of the proposed method by testing its ability to detect several well-documented flash droughts in different regions of the world. The approach successfully identifies (a) a severe flash drought in southwestern Russia and eastern Ukraine that rapidly intensified during late April and early May 2010 (see Supplementary Fig. 2, consistent with findings by refs. 44,45), (b) one of the most severe flash droughts experienced in India occurred at the end of the 2001 monsoon season (see Supplementary Fig. 3, in agreement with ref. 46), and (c) the extremely rapid intensification and spatiotemporal evolution of the once-a-century 2013 flash drought in southern China (see Supplementary Fig. 4, in line with the studies by refs. 47,48).

Annual and seasonal frequencies of agricultural flash drought

Our approach is employed to estimate the global spatial distribution of agricultural flash drought frequencies over the 1960–2020 period. Regions with the highest annual frequency of agricultural flash drought events are identified as hotspots, that is, regions where agricultural flash droughts have an area-averaged frequency higher than two events per decade and in which half of the area experiences at least three events per decade. Eight world regions prone to high agricultural flash drought occurrence are identified with the proposed method. These regions, highlighted in Fig. 3a, are presented in Table 1 along with the corresponding flash drought frequencies. Southern China (SCh), central-eastern Europe (CEEu), India (In), southeastern South America (SESA), and southern Russia (SRus) present the highest frequencies per decade (with area-averaged frequencies between 3.3 and 2.8 events per decade). Central-eastern USA (CEUSA) shows a lower area-averaged frequency (2.3 events per decade) but an extended area that experiences more than three events per decade (see Fig. 3a). Lastly, the transition belt between the Sahel and the tropical forests in central-western Africa (CWAf), northern South America (NSA), and southeastern Asia (SEAs) are also identified as agricultural flash drought hotspots with area-

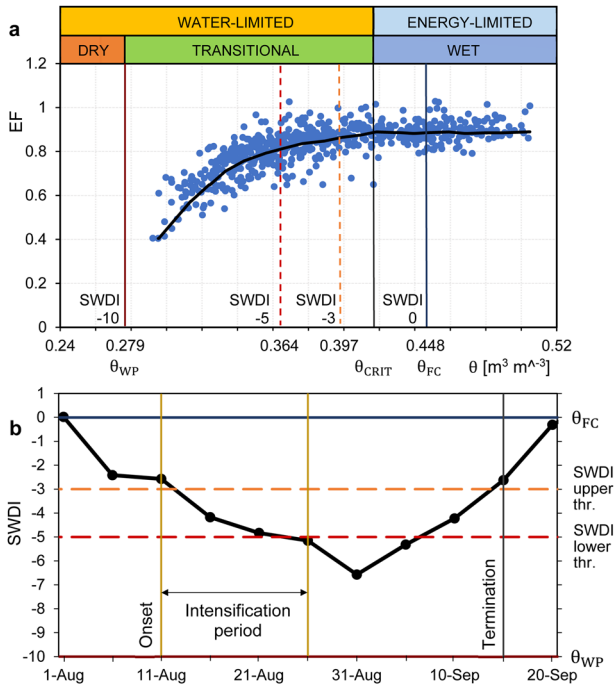

Fig. 1 | Illustration of the proposed agricultural flash drought definition. **a** Scatterplot of evaporative fraction (EF) vs. volumetric soil moisture (θ) at the grid point corresponding to the agricultural flash drought case presented in **b** (adapted from refs. 10,32). The blue dots represent the pentad values from 1 Aug–20 Sep during the 1960–2020 period. The black line represents the average EF-θ relationship computed by binning the data within θ ranges close to 0.01 $m^3 m^{-3}$. Soil moisture (dry, transitional, and wet) and evapotranspiration (water- and energy-limited) regimes are highlighted with colors. The solid vertical lines indicate the soil property values, namely permanent wilting point (θ_{WP}), soil moisture critical value (θ_{CRIT}), and field capacity (θ_{FC}) with their corresponding soil water deficit index (SWDI) values. The dashed vertical lines highlight the SWDI thresholds. The upper SWDI threshold (SWDI = −3) is at the beginning of the transitional regime and the lower SWDI threshold (SWDI = −5) ensures that several crops begin to experience water stress. **b** Representative example of an agricultural flash drought case experienced in southern China (112°E, 28°N) during the summer of 2020. The solid black line shows the pentads (5-day means) for the SWDI (left axis) and θ (right axis) during the flash drought event. The upper and lower SWDI thresholds are shown as dashed lines, while θ_{FC} and θ_{WP} are presented as solid lines.

averaged frequencies between 2.3 to 2 events per decade. Notably, the most prominent event frequencies occur in croplands (Supplementary Figs. 5 and 6) of SCh, CEEu and SRus, central In, SESA, and the northern and southeastern portions of the CEUSA (Fig. 3a).

While the number of area-averaged cases is seemingly low, they encompass smaller regions with frequent agricultural flash droughts (Fig. 3a). SCh, In, SESA, and SEAs present small regions with frequencies of more than eight events per decade, where also a few grid points show maximum frequencies approaching or exceeding one flash drought event per year (Table 1). Large regions of SRus and the eastern CEEu and isolated areas of CEUSA and NSA experience between 5 and 8 events per decade.

Agricultural flash droughts tend to occur during the critical growth period of crops according to the analysis of their seasonal frequency (Fig. 3b, c). In extratropical areas, agricultural flash droughts are most frequent in springtime (Fig. 3b). Central-eastern Europe and southern Russia have the most prominent flash drought event frequencies during boreal spring (March–April–May; MAM), thus impacting the planting and pollination periods of diverse rainfed crops, including wheat, barley, corn, soybeans, and rice (see Supplementary Fig. 6b). The main crops grown in the southern USA eastern seaboard and the midwestern USA corn belt (e.g., ref. 49) are impacted during the same season (MAM), with effects extending into June for the latter region. Last, in southeastern South America, agricultural flash droughts are most frequent in austral spring (November and December), thus impacting the planting and pollination periods of corn, soybean, and sunflower (see, e.g., ref. 50).

In subtropical and tropical regions, the highest agricultural flash drought frequency may occur during the spring and summer seasons (Fig. 3b). In southern China, the maximum flash drought frequency occurs during boreal summer (July and August, Fig. 3c), thus reducing the water availability for rice cultivation in an area that concentrates most of the country's rice production[51]. Agricultural flash droughts in India, southeastern Asia, and central-western Africa are most frequent during September-October-November (SON), affecting the main crop yields (e.g., refs. 46,52,53). In the croplands of northern South America (Colombia and Venezuela), frequent flash drought events in December-January-February (DJF) affect the critical growth periods of mixed crops, cotton, and coffee (Supplementary Fig. 6b, ref. 54).

Physical evolution of agricultural flash droughts

Analyzing the temporal progression of agricultural flash droughts helps understand the physical processes involved in their life cycle and the associated land-atmosphere feedbacks. All hotspot regions under agricultural flash drought conditions exhibit a similar temporal evolution of the area-averaged standardized anomalies of relevant variables (Fig. 4), suggesting worldwide analogous agricultural flash drought life cycle. The generic spatial structure of agricultural flash droughts (Fig. 5) reveals a consistent spatiotemporal flash drought development. Before the agricultural flash drought onset (lags −4 to −1), temperature has almost constant values and precipitation slightly decreases (Fig. 4a, b). As non-drought conditions persist within the energy-limited regime (refer to Fig. 1b) during this phase, sufficient soil moisture (Fig. 4d) allows a slight increase in evapotranspiration (Fig. 4c). Between the lag −1 and the onset, precipitation quickly decays while the temperature rises (Fig. 4a,b; 5, first and second columns). At this point, an enhanced evaporative demand favored by the warming rapidly increases evapotranspiration (Figs. 4c and 5, third column). Together with the precipitation decay, this increased evapotranspiration produces a soil moisture dry-down that accelerates over the following pentads.

At the flash drought onset (lag = 0), when the SWDI is above the upper threshold (SWDI = −3; Figs. 4e and 5, fifth column), the precipitation deficit deepens, and the soil moisture starts depleting (Figs. 4a, d; 5, first and fourth columns). At this time, temperature and evapotranspiration play a crucial role in flash drought development. After the flash drought onset (lag +1), the precipitation deficit reaches its maximum intensity and extent (Fig. 5, first column) and soil moisture becomes insufficient to supply further water for evapotranspiration, signaling the start of the water-limited conditions (see Fig. 1b). From lag +1, evapotranspiration starts to decrease, despite the increased temperature, due to water stress (Figs. 4c and 5, third column). As the flash drought progresses (lags +1 to +3), the mechanism intensifies, that is, the temperature continues to rise, evapotranspiration drops, and soil moisture diminishes. By lag +2 the precipitation deficit begins stabilizing and reverses slightly by lag +3, although negative precipitation anomalies persist (Figs. 4a and 5, first column). At this time (lag +3), the temperature starts to drop (while positive anomalies continue), and the negative anomalies of both evapotranspiration and soil moisture stabilize, indicating the approaching end of the flash drought intensification period.

The characteristics just described are notably seen in all regions with agricultural flash droughts, regardless of the location or climatic regime. The features are more marked in the main hotspots (SCh, CEEu and SRus, In, SESA, and CEUSA), where the largest negative precipitation anomalies and the highest positive evapotranspiration anomalies occur (see Supplementary Fig. 7).

Discussion

Flash droughts are challenging to predict, but we can better understand their development by identifying common features across all regions. We have introduced an approach to recognize agricultural flash droughts based on

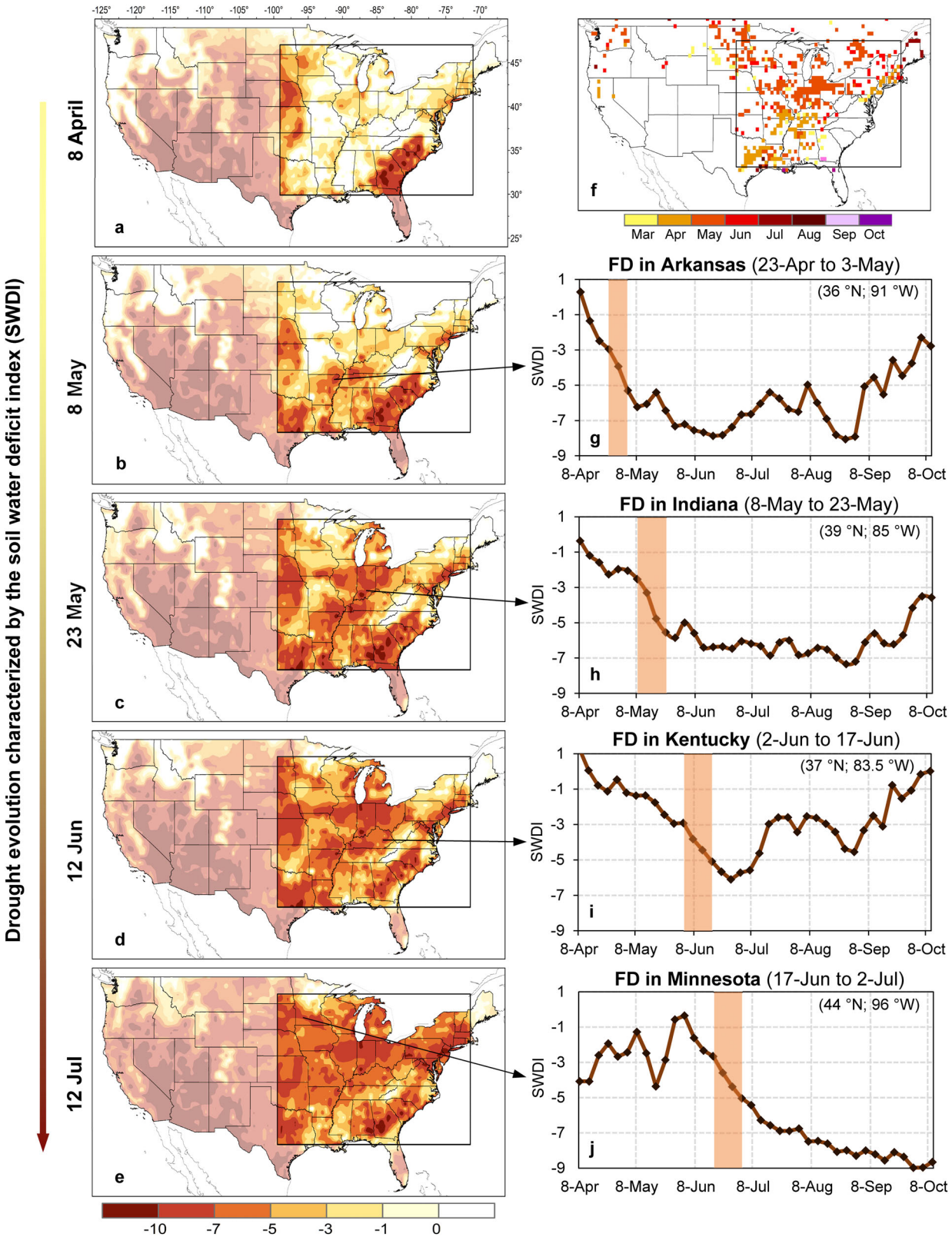

Fig. 2 | Evolution of the 2012 flash drought in the central-eastern United States characterized by the proposed SWDI-based indicator. a–e Spatial distribution of the SWDI on key dates during the flash drought evolution. The impacted area in the central-eastern United States stands out. The rest of the country is shown opaqued. **f** Onset months of grid points under agricultural flash droughts in 2012. **g–j** Temporal evolution of the SWDI at selected grid points (referenced in the upper right corner of each panel). The flash drought's intensification period is emphasized in brown shading.

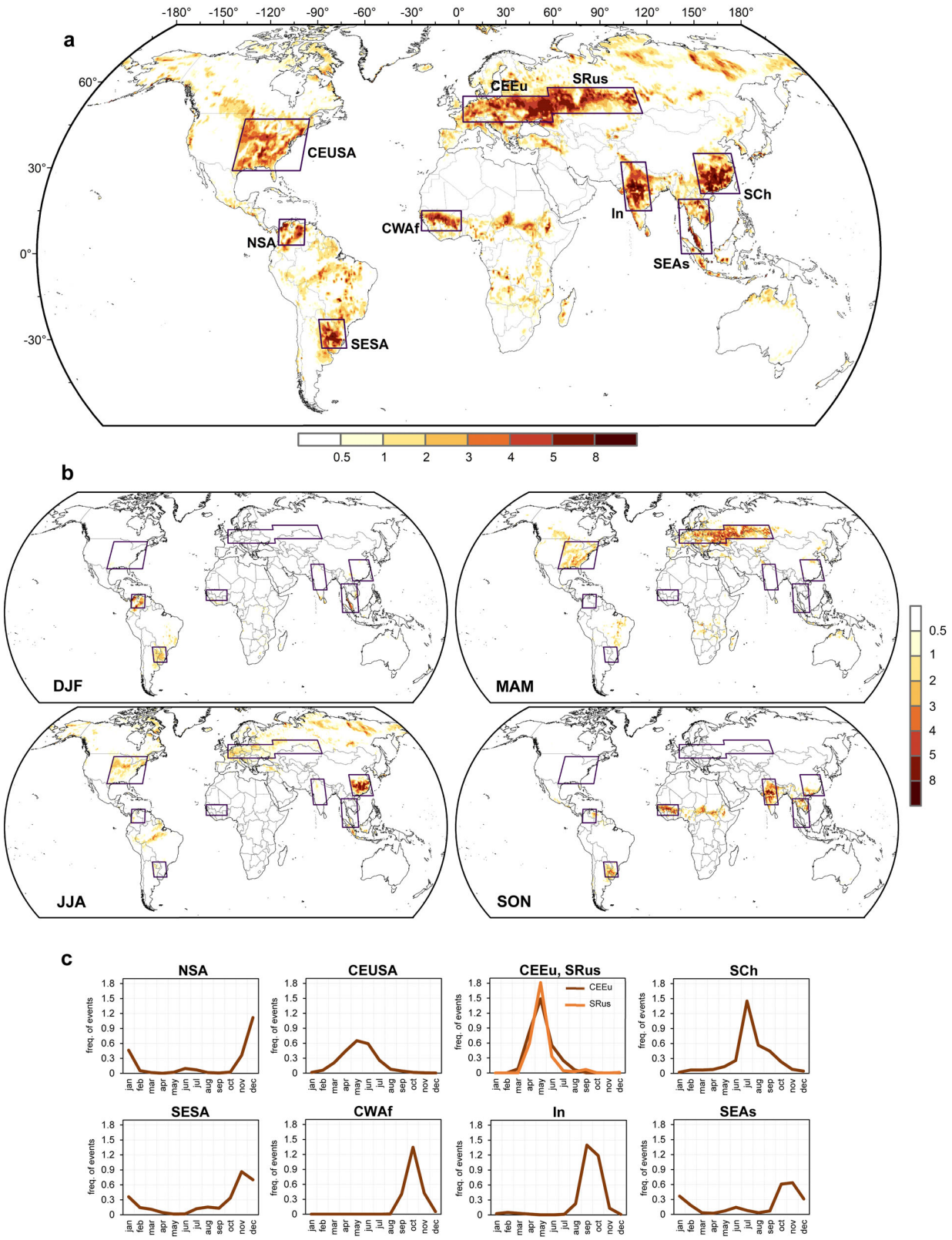

Fig. 3 | Annual and seasonal agricultural flash drought frequencies. a Annual and **b** seasonal frequency of agricultural flash drought events (number of events per decade) from 1960–2020. Meteorological seasons are December-January-February (DJF), March-April-May (MAM), June-July-August (JJA), and September-October-November (SON). Hotspots are highlighted with boxes, including northern South America (NSA), central-eastern United States of America (CEUSA), central-eastern Europe (CEEu) and southern Russia (SRus), southern China (SCh), southeastern South America (SESA), central-western Africa (CWAf), India (In), and southeastern Asia (SEAs). **c** Annual cycles of the area-averaged agricultural flash drought frequency in each hotspot.

Table 1 | Regions identified as agricultural flash drought occurrence hotspots

Hotspot	Acronym	Area-averaged FD frequency	Maximum FD frequency
Southern China	SCh	3.3	12.5
Central-eastern Europe	CEEu	3.2	8.2
India	In	3	9.7
Southeastern South America	SESA	2.9	10.1
Southern Russia	SRus	2.8	8.3
Central-eastern United States of America	CEUSA	2.3	7.7
Southeastern Asia	SEAs	2.3	10.6
Northern South America	NSA	2.1	8.5
Central-western Africa	CWAf	2	8.5

The columns show the acronyms used to identify the agricultural flash drought hotspots and the area-averaged and maximum decadal frequencies of flash droughts (FD) in each hotspot. Even though CEUSA and SRus frequencies are displayed separately, both regions represent a unified hotspot region (see Fig. 3a).

soil water availability. The method utilizes the root-zone soil moisture and two soil hydraulic properties, namely field capacity and wilting point, to capture the rapid depletion of soil moisture, along with vegetation stress that severely impacts agriculture and ecosystems. To detect such occurrences, we suggest using the well-known SWDI along with a threshold range within the transitional regime. The upper SWDI threshold marks the initiation of the soil moisture deficit, while the lower SWDI threshold indicates water stress conditions on crops (see Supplementary Fig. 8).

We utilized the ERA5 dataset for our study, but it should be noted that this dataset has some known uncertainties[55]. While we acknowledge that there are also inaccuracies in estimating soil hydraulic properties and that these estimates may not be representative in certain regions[56,57], our approach correctly identifies several well-known flash drought events across the globe. It's important to note that different definitions of flash droughts and the use of varying input data can lead to differences in the occurrence, intensity, onset, intensification period, and drivers of these events[30,31]. Our method relies on soil moisture and soil-specific water availability, aligning our findings more closely with studies that use soil moisture indicators at either global scales[9,14] or regional scales (such as in China[25] and India[58]), rather than evapotranspiration indicators[5,11,21,27]. Additionally, it's worth noting that our method is specifically designed to identify agricultural flash droughts, and therefore excludes flash droughts that occur in soils and climates that are less suitable for agriculture.

Agricultural flash droughts are most frequent in croplands of southern China, central-eastern Europe, southern Russia, India, southeastern South America, and the central-eastern USA. These types of droughts are more common during the critical growth periods of crops. This finding aligns with the underlying mechanisms, as the transition from an energy-limited regime to a water-limited regime is more likely to occur during the growing season when evaporative demand is at its highest climatological levels[2,42]. When this transition takes place, the vegetation becomes stressed quickly, and the impact of agricultural flash droughts is magnified[2,11].

Our study finds that agricultural flash droughts exhibit similar evolution of relevant atmospheric and surface variables regardless of the geographical location or climatic regime. As expected, a precipitation deficit is the main driver for rapid soil moisture depletion. Before the flash drought onset, there is sufficient soil moisture (energy-limited regime). The favorable conditions of abundant soil moisture, combined with a decrease in precipitation, allow evapotranspiration to increase considerably, intensifying and accelerating soil moisture depletion. During the flash drought's intensification period, soil moisture becomes insufficient to supply more water for evapotranspiration, which in turn decreases. In this water-limited regime with decreased evapotranspiration, energy is transferred to sensible heat flux[11,59], i.e., to an increase in temperature that is crucial in the persistence of flash drought events and which may conduct to subsequent heat waves[44].

Methods

Data

The primary variable used in this study was the root-zone volumetric soil moisture in the soil's top meter. Soil moisture data representing the 1960–2020 period at a 0.5° × 0.5° latitude–longitude grid spacing was obtained from the ERA5 product55,60. ERA5 soil moisture data has shown better accuracy than data from other reanalyses compared to in-situ observations at various locations around the world[61,62]. The evaporative fraction, EF = LH/(LH + SH), was estimated from ERA5's latent heat (LH) and sensible heat (SH). Total precipitation, evapotranspiration, and 2-m air temperature were also used. Non-overlapped pentads (5-day means) of these variables were computed from the original hourly data. The pentad values were then used to assess the spatiotemporal evolution of flash droughts' main variables. Such a method avoids higher-frequency variabilities while capturing short-duration flash droughts[15,24]. The pentad anomalies at each grid point were computed as departures from the 1960–2020 mean annual cycle and normalized with their corresponding standard deviations. Such standardized anomalies facilitate worldwide comparisons.

The proposed flash drought definition also employed ERA5 parameters representing soil hydraulic properties. These parameters included the field capacity (θ_{FC}) and the wilting point (θ_{WP}). Both parameters depend on the soil class at each grid point and do not vary temporally. The global soil datasets needed by Earth System Models are often based on limited and heterogeneously distributed soil profiles (e.g., refs. 63,64). The soil properties also present uncertainty due to the pedotransfer functions used in their estimation[65]. However, significant efforts have been made in recent decades to mitigate these limitations. Information on the uncertainty is commonly provided along with the soil datasets (e.g., refs. 66,67), thereby enhancing the accuracy of Earth System Models' land component.

Vegetation types were employed to identify the dominant land cover in agricultural flash drought-prone regions. These vegetation types were defined in ERA5 as a percentage of high and low vegetation coverage for each grid point following the Global Land Cover Characteristics data[68] of the Biosphere-Atmosphere Transfer Scheme biome classification[69]. Our interest focused on discussing the impacts of agricultural flash droughts on croplands. For this reason, the ERA5 data were complemented with products representing the cropland extent, irrigated vs. rainfed crops, and crop dominance. These products were taken from the Global Food Security-Support Analysis Data (GFSAD) Project: The Global Cropland-extent product at a 30-m resolution[70] and the Global Cropland-extent 1-km Cropland Dominance product[71].

Proposed agricultural flash drought definition

The main features of the proposed method for identifying agricultural flash droughts are discussed in the Results section (see "Overview of the proposed method to detect agricultural flash droughts"). Complementary, this section discusses the selection of thresholds and the pros and cons of the proposed method.

Selection of SWDI thresholds. The choice of SWDI = −3 as the upper threshold reflects the fact that this value is less than the θ_{CRIT} value, which determines the beginning of the transitional regime (see Fig. 1a and Supplementary Fig. 1). By setting the upper threshold within the transitional regime, it ensures a discernible reduction in evapotranspiration, effectively capturing the moisture deficit in the land system. The θ_{CRIT} value may be difficult to establish because of the vast influence of varying soil textures, climate conditions, and vegetation characteristics. Reference 72 reported that it is typically 50–80% of θ_{FC}.

The fraction of available water content a plant can extract from the root zone without suffering water stress is known as the readily available soil

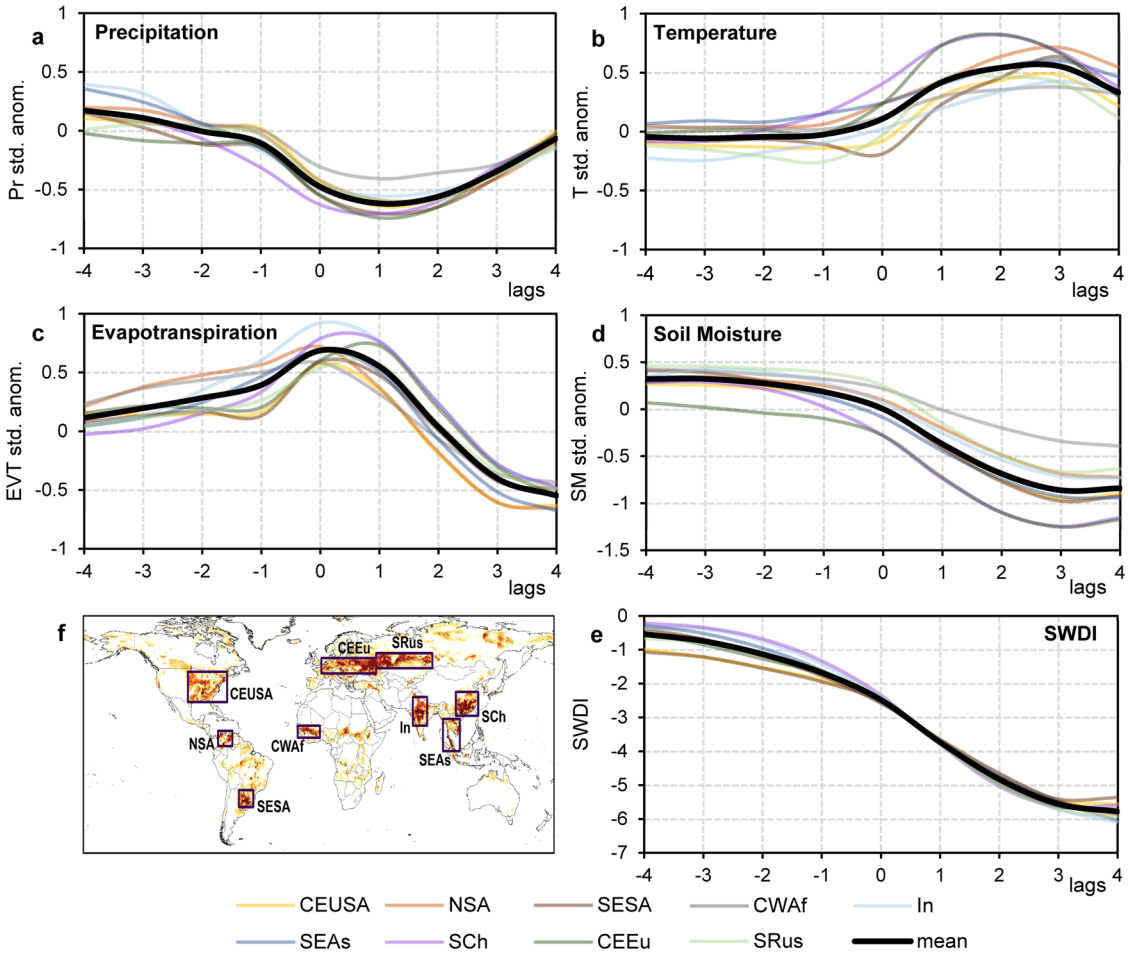

Fig. 4 | Temporal evolution of area-averaged standardized anomalies during agricultural flash drought events. The temporal evolution is shown for the nine-pentad period centered at FD onset (lag = 0) for: **a** precipitation (Pr), **b** temperature (T), **c** evapotranspiration (EVT), and **d** soil moisture (SM). **e** Shows the temporal evolution of the soil water deficit index (SWDI). **f** Map that highlights the agricultural flash drought hotspots. The colored lines represent the individual hotspots. The average value over all hotspots is shown as a thick black line. The full names of the agricultural flash drought hotspots are presented in Table 1.

water[73]. An average fraction of available water content close to 0.5, corresponding to SWDI = −5, is a common feature of several crops[73,74]. Thus, below the SWDI = −5 threshold, plant roots can no longer extract soil water rapidly enough to respond to the transpiration demand, and plants begin to experience water stress. Although soil water is theoretically available for plants before reaching θ_{WP}, the plant water uptake is reduced well before that value (see Supplementary Fig. 8). In addition, ref. 36 classify soil moisture droughts below the SWDI = −5 threshold as severe.

Although the thresholds have been defined based on physical constraints, the precise values have some arbitrariness. Thus, we tested the sensitivity of the threshold range by modifying threshold values and examining their influence on drought frequency results (see Supplementary Fig. 9). The flash drought occurrence patterns remain unaffected across varied threshold ranges, although the frequency of events fluctuates, suggesting that the proposed method is robust. Specifically, flash drought frequencies increase for less stringent ranges (e.g., exceeding five events per decade in larger regions when $-4 < SWDI < -2$) and significantly decrease for more stringent ranges (e.g., fluctuating between 2 and 4 events per decade for $-6 < SWDI < -3$). The chosen range ($-5 < SWDI < -3$), positioned at an intermediate level, was selected based on physical criteria (as discussed above), thereby mitigating the arbitrariness associated with range selection. In addition, the selected thresholds allow proper recognition of the spatiotemporal evolution of several well-documented flash drought events that are distinguished using other definitions in different world regions (e.g., refs. 16,41,44,46; see also Results).

Comparison of the SWDI-based method with an *θ* percentile-based method. We compared the characteristics of agricultural flash droughts identified in this article with flash droughts obtained with a widely used indicator based on root-zone soil moisture percentiles (e.g., refs. 24,25) (see Supplementary Fig. 10). Note that the soil moisture percentile method has also been used with additional constraints to ensure soil moisture stress on the land system, account for prior non-drought conditions, or address cases in extreme climates (see, e.g., ref. 10). However, the comparison conducted here was restricted to the original soil moisture percentile method.

Flash drought identification under extreme climates presents interesting differences between the two approaches. To illustrate this, we examined a grid point in a hot desert climate (Case 1, Sahara Desert; Supplementary Fig. 10a, b) where agricultural flash droughts would not be feasible under these circumstances. Still, the time series of θ percentiles from 2015 to 2020 (Supplementary Fig. 10a) suggests repeated flash drought conditions, as θ frequently decreases from at least 40th to the 20th percentile within four pentads or less. In contrast, the SWDI time series (Supplementary Fig. 10b) indicates that soil moisture fluctuates within a narrow range consistently well below the wilting point throughout the five years. This means that the soil remains under conditions of permanent dryness. An equivalent situation is observed in a very wet climate (Case 2, Indonesia, Supplementary Fig. 10c, d). The θ percentiles time series (Supplementary Fig. 10c) suggests the existence of flash drought conditions. However, the SWDI time series (Supplementary Fig. 10d) reveals that soil moisture varies in a small range always around the field capacity, never reaching the drought

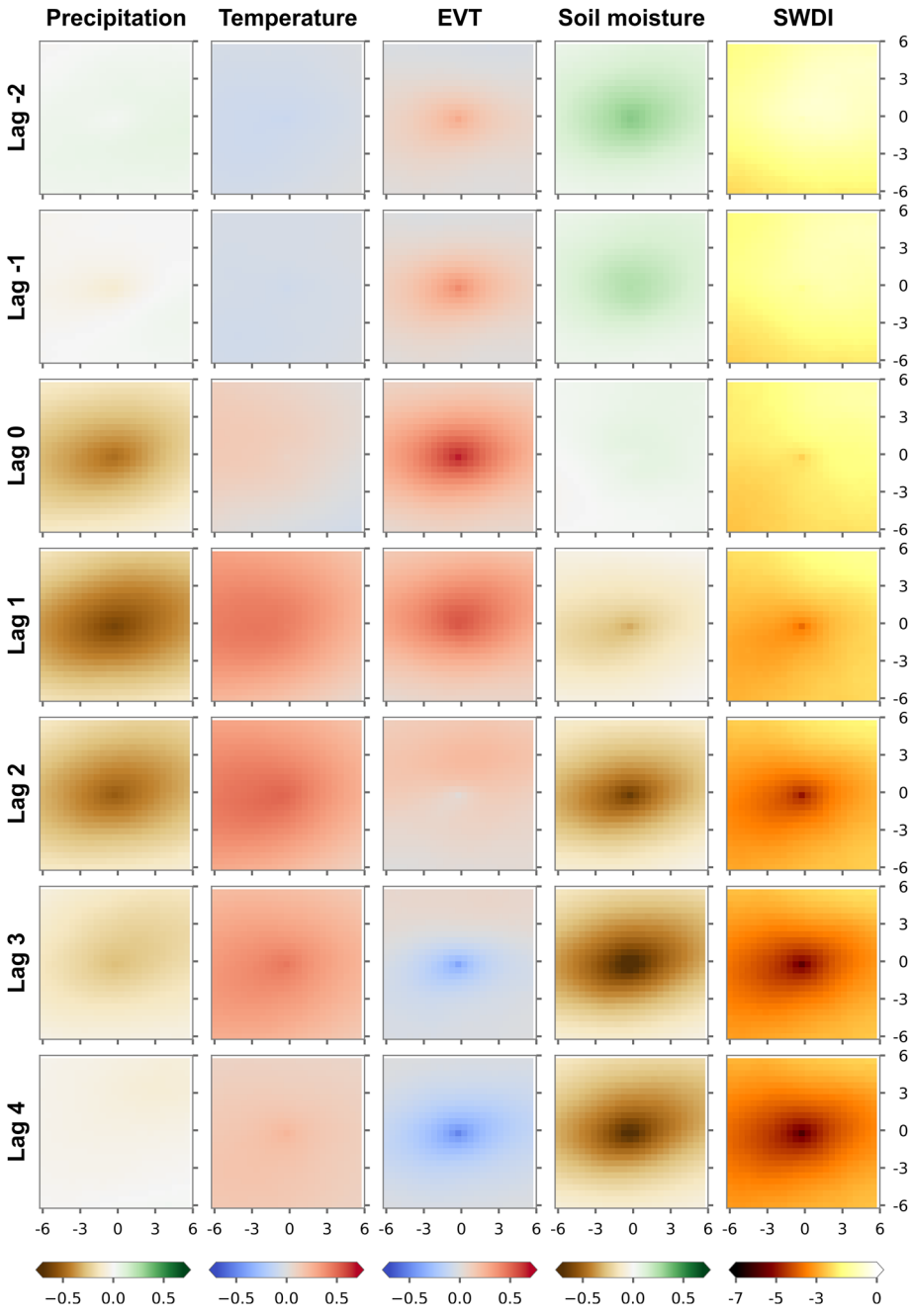

Fig. 5 | Key atmospheric and surface variables that influence agricultural flash drought events before, during, and after their onset. For each variable and each lag, each box represents the composite of all flash drought events for a 12° × 12° window with the event occurring in the center. The lags vary between −2 and +4 around the onset (lag 0). From left to right, the variables are standardized anomalies of precipitation, temperature, evapotranspiration (EVT), and soil moisture. The rightmost column shows the evolution of the soil water deficit index (SWDI).

onset threshold (SWDI < −3), recognizing that there is no plant water stress, and therefore, no drought periods. These results suggest that identifying soil moisture flash droughts based on physical thresholds helps avoid misrepresentation in extreme climates.

We also studied flash drought cases in agricultural-suitable non-extreme climates, aligning with the indicator's focus on agricultural droughts (Supplementary Fig. 10e–h). Case 3 shows a flash drought event in southern China during Aug-Sep 2020 (as in Fig. 1), characterized by the evolution of the θ percentiles (Supplementary Fig. 10e) and by the SWDI and θ time series (Supplementary Fig. 10f). The SWDI-based approach identifies a flash drought of shorter duration and lower intensity than the one estimated from the θ percentile thresholds. Case 4 presents a flash drought event in southeastern South America during Nov-Dec 1970. Both definitions (Supplementary Fig. 10g, h) identify a flash drought of similar duration, but the proposed method in this study indicates a higher intensity. These examples demonstrate that both the SWDI-based and θ percentile-based methods identify similar characteristics of soil moisture flash droughts with slight differences. The θ percentile-based indicators' thresholds may be sensitive to soil moisture variabilities in non-extreme climate regimes. The thresholds of the SWDI-based method are based on the physical conditions of each type of soil.

Evolution of crucial atmospheric and surface variables

Composites of precipitation, temperature, evapotranspiration, and soil moisture standardized anomalies were constructed to examine agricultural flash droughts' characteristic temporal and spatial evolution. First, flash drought events were detected at each grid point within the hotspots. Then, area averages for all hotspots were computed for their onset (lag 0), the four preceding pentads (lags −4 to −1), and the four subsequent pentads (lags +1 to +4). Next, the spatial structure of standardized anomalies across all identified events worldwide was examined by generating a flash drought composite over a 12° × 12° window centered on each event location.

Data availability

The ERA5 data are available at https://doi.org/10.24381/cds.adbb2d47. The Global Cropland-extent product at a 30-m resolution and the Global Cropland-extent 1-km Cropland Dominance product can be obtained from https://doi.org/10.3133/pp1868 and https://doi.org/10.5067/MEaSUREs/GFSAD/GFSAD1KCD.001, respectively.

Code availability

Python scripts for running the proposed method and performing calculations are available at https://github.com/mjpierrestegui/flash-droughts.git.

Received: 14 September 2023; Accepted: 7 March 2024;
Published online: 19 March 2024

References

1. Svoboda, M. et al. The drought monitor. *Bull. Am. Meteor. Soc.* **83**, 1181–1190 (2002).
2. Otkin, J. et al. Flash droughts: a review and assessment of the challenges imposed by rapid onset droughts in the United States. *Bull. Am. Meteor. Soc.* **99**, 911–919 (2018).
3. Yuan, X. et al. A global transition to flash droughts under climate change. *Science* **380**, 187–191 (2023).
4. Sreeparvathy, V. & Srinivas, V. V. Meteorological flash droughts risk projections based on CMIP6 climate change scenarios. *npj Clim. Atmos. Sci.* **5**, 77, https://doi.org/10.1038/s41612-022-00302-1 (2022).
5. Christian, J. I. et al. Global projections of flash drought show increased risk in a warming climate. *Commun. Earth. Environ.* **4**, 165, https://doi.org/10.1038/s43247-023-00826-1 (2023).
6. Otkin, J. A. et al. Getting ahead of flash drought: from early warning to early action. *Bull. Am. Meteor. Soc.* **103**, E2188–E2202, https://doi.org/10.1175/BAMS-D-21-0288.1 (2022).
7. He, M. et al. Impacts of the 2017 flash drought in the US Northern plains informed by satellite-based evapotranspiration and solar-induced fluorescence. *Environ. Res. Let.* **14**, 074019 (2019).
8. Yao, T., Liu, S., Hu, S. & Mo, X. Response of vegetation ecosystems to flash drought with solar-induced chlorophyll fluorescence over the Hai River Basin, China during 2001–2019. *J. Environ. Manag.* **313**, 114947 (2022).
9. Mahto, S. S. & Mishra, V. Increasing risk of simultaneous occurrence of flash drought in major global croplands. *Environ. Res. Lett.* **18**, 044044 (2023).
10. Koster, R. D., Schubert, S. D., Wang, H., Mahanama, S. P. & DeAngelis, A. M. Flash drought as captured by reanalysis data: Disentangling the contributions of precipitation deficit and excess evapotranspiration. *J. Hydrometeor.* **20**, 1241–1258 (2019).
11. Pendergrass, A. G. et al. Flash droughts present a new challenge for subseasonal-to-seasonal prediction. *Nat. Clim. Chang.* **10**, 191–199 (2020).
12. Liu, L. et al. Soil moisture dominates dryness stress on ecosystem production globally. *Nat. Commun.* **11**, 4892 (2020).
13. Zhang, M. & Yuan, X. Rapid reduction in ecosystem productivity caused by flash droughts based on decade-long FLUXNET observations. *Hydrol. Earth Syst. Sci.* **24**, 5579–5593 (2020).
14. Mukherjee, S. & Mishra, A. K. A multivariate flash drought indicator for identifying global hotspots and associated climate controls. *Geophys. Res. Lett.* **49**, e2021GL096804 (2022).
15. Mo, K. C. & Lettenmaier, D. P. Heat wave flash droughts in decline. *Geophys. Res. Lett.* **42**, 2823–2829 (2015).
16. Basara, J. B. et al. The evolution, propagation, and spread of flash drought in the Central United States during 2012. *Environ. Res. Lett.* **14**, 084025 (2019).
17. Nguyen, H., Wheeler, M. C., Otkin, J. A., Nguyen-Huy, T. & Cowan, T. Climatology and composite evolution of flash drought over Australia and its vegetation impacts. *J. Hydrometeor.* **24**, 1087–1101 (2023).
18. Wang, Y. & Yuan, X. Land-atmosphere coupling speeds up flash drought onset. *Sci. Total Environ.* **851**, 158109 (2022).
19. Mahto, S. S., & Mishra, V. Flash drought intensification due to enhanced land-atmospheric coupling in India. *J. Clim.* 1–31, https://doi.org/10.1175/JCLI-D-22-0477.1 (2023).
20. Osman, M. et al. Diagnostic classification of flash drought events reveals distinct classes of forcings and impacts. *J. Hydrometeor.* **23**, 275–289 (2022).
21. Christian, J. I. et al. Global distribution, trends, and drivers of flash drought occurrence. *Nat. Commun.* **12**, 6330 (2021).
22. Lowman, L. E. L., Christian, J. I. & Hunt, E. D. How land surface characteristics influence the development of flash drought through the drivers of soil moisture and vapor pressure deficit. *J. Hydrometeor.* **24**, 1395–1415 (2023).
23. Lisonbee, J., Woloszyn, M. & Skumanich, M. Making sense of flash drought: definitions, indicators, and where we go from here. *J. Appl. Serv. Climatol.* **2021**, 1–19 (2021).
24. Ford, T. W. & Labosier, C. F. Meteorological conditions associated with the onset of flash drought in the eastern United States. *Agric. Meteor.* **247**, 414–423 (2017).
25. Yuan, X. et al. Anthropogenic shift towards higher risk of flash drought over China. *Nat. Commun.* **10**, 1–8 (2019).
26. Liu, Y. et al. Two different methods for flash drought identification: comparison of their strengths and limitations. *J. Hydrometeor.* **21**, 691–704 (2020).
27. Christian, J. I. et al. A methodology for flash drought Identification: application of flash drought frequency across the United States. *J. Hydrometeor.* **20**, 833–846 (2019).
28. Hobbins, M. T. et al. The evaporative demand drought index. Part I: Linking drought evolution to variations in evaporative demand. *J. Hydrometeor*. **17**, 1745–1761 (2016).
29. Li, J. et al. A voxel-based three-dimensional framework for flash drought identification in space and time. *J. Hydrol.* **608**, 127568 (2022).
30. Osman, M. et al. Flash drought onset over the contiguous United States: sensitivity of inventories and trends to quantitative definitions. *Hydrol. Earth Syst. Sci.* **25**, 565–581 (2021).
31. Mukherjee, S. & Mishra, A. K. Global flash drought analysis: uncertainties from indicators and datasets. *Earth's Future* **10**, e2022EF002660 (2022).
32. Seneviratne, S. I. et al. Investigating soil moisture–climate interactions in a changing climate: a review. *Earth. Sci. Rev.* **99**, 125–161 (2010).
33. Van Loon, A. F. Hydrological drought explained. *Wiley Interdiscip. Rev. Water* **2**, 359–392 (2015).
34. Hillel, D. *Environmental Soil*. *Physics*. (Academic Press, San Diego, 1998).
35. Kirkham, M. B Field capacity, wilting point, available water, and the non-limiting water range. In *Principles of Soil and Plant Water Relations* 101–115 (Academic Press, Burlington, 2005).
36. Martínez-Fernández, J., González-Zamora, A., Sánchez, N. & Gumuzzio, A. A soil water-based index as a suitable agricultural drought indicator. *J. Hydrol.* **522**, 265–273 (2015).
37. Savage, M. J., Ritchie, J. T., Bland, W. L. & Dugas, W. A. Lower limit of soil water availability. *Agron. J.* **88**, 644–651 (1996).
38. Fu, Z. et al. Critical soil moisture thresholds of plant water stress in terrestrial ecosystems. *Sci. Adv.* **8**, eabq7827 (2022).
39. Koster, R. D. et al. Regions of strong coupling between soil moisture and precipitation. *Science* **305**, 1138–1140 (2004).
40. Seneviratne, S. I., Lüthi, D., Litschi, M. & Schär, C. Land–atmosphere coupling and climate change in Europe. *Nature* **443**, 205–209 (2006).
41. Otkin, J. A. et al. Assessing the evolution of soil moisture and vegetation conditions during the 2012 United States flash drought. *Agric. Meteorol.* **218-219**, 230–242 (2016).
42. Otkin, J. A. et al. Development of a Flash Drought Intensity Index. *Atmosphere* **12**, 741 (2021).

43. Jin, C., Luo, X. & Xiao, X. et al. The 2012 flash drought threatened US Midwest Agroecosystems. *Chin. Geogr. Sci.* **29**, 768–783 (2019).
44. Christian, J. I., Basara, J. B., Hunt, E. D., Otkin, J. A. & Xiao, X. Flash drought development and cascading impacts associated with the 2010 Russian heatwave. *Environ. Res. Lett.* **15**, 094078 (2020).
45. Hunt, E. D. et al. Agricultural and food security impacts from the 2010 Russia flash drought. *Weather Clim. Extrem.* **34**, 100383 (2021).
46. Mahto, S. S. & Mishra, V. Dominance of summer monsoon flash droughts in India. *Environ. Res. Lett.* **15**, 104061 (2020).
47. Yuan, X., Ma, Z., Pan, M. & Shi, C. Microwave remote sensing of short-term droughts during crop growing seasons. *Geophys. Res. Lett.* **42**, 4394–4401 (2015).
48. Zhang, L. et al. Analysis of flash droughts in China using machine learning. *Hydrol. Earth Syst. Sci.* **26**, 3241–3261 (2022).
49. Mishra, V. & Cherkauer, K. A. Retrospective droughts in the crop growing season: implications to corn and soybean yield in the Midwestern United States. *Agric. Meteorol.* **150**, 1030–1045 (2010).
50. Sgroi, L. C., Lovino, M. A., Berbery, E. H. & Müller, G. V. Characteristics of droughts in Argentina's Core Crop Region. *Hydrol. Earth Syst. Sci.* **25**, 2475–2490 (2021).
51. Deng, N. et al. Closing yield gaps for rice self-sufficiency in China. *Nat. Commun.* **10**, 1725 (2019).
52. Sultan, B., Defrance, D. & Iizumi, T. Evidence of crop production losses in West Africa due to historical global warming in two crop models. *Sci. Rep.* **9**, 12834 (2019).
53. Venkatappa, M., Sasaki, N., Han, P. & Abe, I. Impacts of droughts and floods on croplands and crop production in southeast Asia: an application of Google Earth engine. *Sci. Total Environ.* **795**, 148829 (2021).
54. Geng, G. et al. Agricultural drought hazard analysis during 1980–2008: a global perspective. *Int. J. Climatol.* **36**, 389–399 (2016).
55. Hersbach, H. et al. The ERA5 global reanalysis. *Q. J. R. Meteorol. Soc.* **146**, 1999–2049 (2020).
56. Hengl, T. et al. SoilGrids1km—Global soil information based on automated mapping. *PLOS One* **9**(8), e105992, https://doi.org/10.1371/journal.pone.0105992 (2014).
57. Folberth, C. et al. Uncertainty in soil data can outweigh climate impact signals in global crop yield simulations. *Nat. Commun.* **7**, 11872 (2016).
58. Mishra, V., Aadhar, S. & Mahto, S. S. Anthropogenic warming and intraseasonal summer monsoon variability amplify the risk of future flash droughts in India. *NPJ Clim. Atmos. Sci.* **4**, 1–10 (2021).
59. Fischer, E. M., Seneviratne, S. I., Lüthi, D. & Schär, C. Contribution of land–atmosphere coupling to recent European summer heat waves. *Geophys. Res. Lett.* **34**, L06707 (2007).
60. Bell, B. et al. The ERA5 global reanalysis: preliminary extension to 1950. *Q. J. R. Meteorol. Soc.* **147**, 4186–4227 (2021).
61. Li, M., Wu, P. & Ma, Z. A comprehensive evaluation of soil moisture and soil temperature from third-generation atmospheric and land reanalysis data sets. *Int J. Climatol.* **40**, 5744–5766 (2020).
62. Yang, S., Zeng, J., Fan, W. & Cui, Y. Evaluating root-zone soil moisture products from GLEAM, GLDAS, and ERA5 based on in situ observations and triple collocation method over the Tibetan Plateau. *J. Hydrometeor.* **23**, 1861–1878 (2022).
63. Dai, Y. et al. A review of the global soil property maps for Earth system models. *Soil* **5**, 137–158 (2019).
64. Fatichi, S., Or, D. & Walko, R. et al. Soil structure is an important omission in Earth System Models. *Nat. Commun.* **11**, 522 (2020).
65. Szabó, B., Weynants, M. & Weber, T. K. D. Updated European hydraulic pedotransfer functions with communicated uncertainties in the predicted variables (euptfv2). *Geosci. Model Dev.* **14**, 151–175 (2021).
66. Poggio, L. et al. SoilGrids 2.0: producing soil information for the globe with quantified spatial uncertainty. *Soil* **7**, 217–240 (2021).
67. Chen, S. et al. Digital mapping of GlobalSoilMap soil properties at a broad scale: a review. *Geoderma* **409**, 115567 (2022).
68. Loveland, T. R. et al. Development of a global land cover characteristics database and IGB6 DISCover from the 1km AVHRR data. *Int. J. Remote Sens.* **21**, 1303–1330 (2000).
69. Dickinson, R., Henderson-Sellers, A. & Kennedy, P. Biosphere-Atmosphere Transfer Scheme (BATS) Version 1e as Coupled to the NCAR Community Climate model. *Technical Report NCAR/TN-387 + STR* (NCAR Boulder, Colorado, 1993).
70. Thenkabail, P. S. et al. Global cropland-extent product at 30-m resolution (GCEP30) derived from Landsat satellite time-series data for the year 2015 using multiple machine-learning algorithms on Google Earth Engine cloud. *U. S. Geol. Surv. Prof. Pap.* **1868**, 1–63 (2021).
71. Thenkabail, P. S. et al. Assessing future risks to agricultural productivity, water resources and food security: how can remote sensing help? *Photogram. Eng. Remote Sens.* **78**, 773–782 (2012).
72. Shuttleworth, W. J. Evaporation. In *Handbook of Hydrology* 4.1–4.53 (McGraw-Hill Inc, New York, 1993).
73. Allen R.G., Pereira L.S., Raes, D., & Smith M. Crop Evapotranspiration: Guidelines for Computing Crop Water Requirements: Irrigation and Drainage Paper **56** (Food and Agriculture Organization of the United Nations, Rome, 1998).
74. Ceppi, A. et al. Realtime drought forecasting system for irrigation management. *Hydrol. Earth Syst. Sci.* **18**, 3353–3366 (2014).

Acknowledgements

This research was supported by Argentina's National Agency for Scientific and Technological Promotion (Projects PICT-2019-2019-03982 and PICT-2019-2019-00481), the Argentine National Council for Scientific and Technical Research (Grant PIP-CONICET-11220200102257CO), and the Universidad Nacional del Litoral (Grant CAI + D-2020-50620190100082LI). E.H.B. was supported by NOAA grant NA19NES4320002 (Cooperative Institute for Satellite Earth System Studies (CISESS)) at the University of Maryland/ESSIC. E.H.B. thanks the Fulbright Commission for facilitating the last stages of this research.

Author contributions

O.V.M., M.A.L., and E.H.B. designed the study. M.A.L. and M.J.P. carried out the research. M.A.L., M.J.P., O.V.M., G.V.M., and E.H.B. analyzed and discussed the results. M.A.L., G.V.M., and E.H.B. acquired funding and resources. M.A.L. prepared the original manuscript, and all authors contributed to its subsequent versions.

Competing interests

The authors declare no competing interests.

Additional information

Supplementary information The online version contains supplementary material available at https://doi.org/10.1038/s41612-024-00618-0.

Correspondence and requests for materials should be addressed to Miguel A. Lovino.